BASIC SCIENCE

Nanomedicine: Nanotechnology, Biology, and Medicine
14 (2018) 1695–1706

Research Article

nanomedjournal.com

Enhanced antibacterial nanocomposite mats by coaxial electrospinning of polycaprolactone fibers loaded with Zn-based nanoparticles

Gina Prado-Prone, MSc[a,b], Phaedra Silva-Bermudez, PhD[b,*], Argelia Almaguer-Flores, PhD[c], Jorge A. García-Macedo, PhD[d], Victor I. García, PhD[c], Sandra E. Rodil, PhD[e], Clemente Ibarra, PhD[b,f], Cristina Velasquillo, PhD[g,*]

[a]*Posgrado en Ciencia e Ingeniería de Materiales, Universidad Nacional Autónoma de México, Ciudad de México, México*
[b]*Unidad de Ingeniería de Tejidos, Terapia Celular y Medicina Regenerativa, Instituto Nacional de Rehabilitación Luis Guillermo Ibarra Ibarra, Ciudad de México, México*
[c]*División de Estudios de Posgrado e Investigación, Facultad de Odontología, Universidad Nacional Autónoma de México, Ciudad de México, México*
[d]*Instituto de Física, Universidad Nacional Autónoma de México, Ciudad de México, México*
[e]*Instituto de Investigaciones en Materiales, Universidad Nacional Autónoma de México, Ciudad de México, México*
[f]*Dirección General, Instituto Nacional de Rehabilitación Luis Guillermo Ibarra Ibarra, Ciudad de México, México*
[g]*Subdirección de Investigación Tecnológica, Instituto Nacional de Rehabilitación Luis Guillermo Ibarra Ibarra, Ciudad de México, México*

Received 23 October 2017; accepted 7 April 2018

Abstract

ZnO and Zn acetate nanoparticles were embedded in polycaprolactone coaxial-fibers and uniaxial-fibers matrices to develop potential antibacterial nanocomposite wound dressings (mats). Morphology, composition, wettability, crystallinity and fiber structure of mats were characterized. Antibacterial properties of mats were tested against *E. coli* and *S. aureus* by turbidity and MTT assays. The effect of UVA illumination (prior to bacteria inoculation) on mats' antibacterial activity was also studied. Results showed that a coaxial-fibers design maintained nanoparticles distributed in the outer-shell of fibers and, in general, enhanced the antibacterial effect of the mats, in comparison to conventional uniaxial-fibers mats. Results indicated that mats simultaneously inhibited planktonic and biofilm bacterial growth by, probably, two main antibacterial mechanisms; 1) release of Zn^{2+} ions (mainly from Zn acetate nanoparticles) and 2) photocatalytic oxidative processes exerted by ZnO nanoparticles. Antibacterial properties of mats were significantly improved by coaxial-fibers design and exposure to UVA-light prior to bacteria inoculation.

Key words: Antibacterial nanocomposites; ZnO nanoparticles; Zn acetate; Polycaprolactone; Coaxial electrospinning

One of the biggest challenges facing skin injuries treatment are bacterial infections, which have become increasingly difficult to treat due to rapid emergence of antibiotic-resistant bacteria.[1,2] Recently, use of nanoparticles (nps) has emerged as a novel strategy to face this challenge, because, nps usually exhibit enhanced antibacterial activity as compared to corresponding bulk materials.[3] Different zinc compounds exhibit antibacterial activity: Particularly, ZnO nps (ZnOnps), "generally recognized as safe" by the FDA (21CFR182.8991), are effective against Gram-negative and Gram-positive bacteria, including antibiotics-resistant strains.[3–7] ZnOnps antibacterial effects are commonly attributed to: 1) mechanical cell membrane damage,[8] 2) destabilization of bacterial membranes,[5] and 3) oxidative stress.[5,9] Although nps are gaining popularity as antimicrobial agents, there are still concerns about possible long-term

The authors declare that no competing interests are present, and there is no conflict of interest.

Statement of funding: This project was partly funded by CONACyT, Mexico City (PhD scholarship number 443935); Instituto Nacional de Rehabilitación Luis Guillermo Ibarra Ibarra, Mexico City; Instituto de Física, Universidad Nacional Autonoma de Mexico, Mexico City and Instituto de Investigaciones en Materiales, Universidad Nacional Autonoma de Mexico, Mexico City. SER acknowledges support from CONACYT 251279.

A preliminary work related to the research presented in this paper was presented as a talk at the BIOS SPIE 2017.

*Corresponding authors.
E-mail addresses: phaedrasilva@yahoo.com, pssilva@inr.gob.mx (P. Silva-Bermudez), mvelasquillo@inr.gob.mx (C. Velasquillo).

https://doi.org/10.1016/j.nano.2018.04.005
1549-9634/

side effects of their uncontrolled release into human tissues.[5] One method to restrict nps release is to embed them into biocompatible polymeric matrices, such as polycaprolactone (PCL).[10]

In the present work, we developed antibacterial nanocomposites Zn-based nps/PCL fibrillar matrices, aiming to provide a barrier against bacterial adhesion and proliferation during skin wounds treatment. Fibrillar matrices (mats) were obtained by electrospinning of PCL and PCL-ZnOnps solutions; acetic acid (AcAc) was used as a green-solvent potentially less toxic than other solvents used for PCL electrospinning.[11,12] Antibacterial properties of nps mostly depend on available contact area; then, nps trapped in the center of conventionally electrospun uniaxial-fibers do not significantly contribute to mats antibacterial properties but increase nps concentration, and consequently, the amount of nps that might be released upon eventual mats degradation. To optimize superficial nps:PCL ratios and to decrease mats nps concentration, we developed coaxial-fibers mats where the inner-core and outer-shell were filled with PCL and ZnOnps-PCL solutions, respectively. Uniaxial-fibers were electrospun from ZnOnps-PCL solutions.

Antibacterial activity of mats was tested against *Escherichia coli* and *Staphylococcus aureus;* bacteria strains frequently found in infected skin wounds.[13–17] Antibacterial effect of mats exposure to UVA light before bacteria inoculation was also studied.

Methods

Methods are described in detail in Supplementary Material; briefly:

ZnO nanoparticles characterization

ZnOnps (Sigma Aldrich) crystalline structure and average crystal size were determined by X-Ray Diffraction (XRD; Bruker D8). Morphology and size were characterized by Transmission Electron Microscopy (TEM; Philips FEI TECNAI10) and energy gap (Eg) was estimated from UV-Vis absorption spectra (Thermo Spectronic Genesys2) using Eq. (1)[18]:

$$(\alpha h\upsilon)^2 = C(h\upsilon - Eg) \quad (1)$$

where, α, absorption coefficient; $h\upsilon$, photon energy and C depends on electron-hole mobility.

AcAc can react with ZnO to produce zinc acetate ($Zn(CH_3CO_2)_2$); an organic antibacterial compound.[19–22] Thus, ZnOnps were dispersed in AcAc, stirred for 24 h, dried and evaluated by XRD, TEM and Infrared Spectroscopy (FT-IR; Nicolet 6706/Smart Orbit ATR optics) (data not shown) to aid in present results analysis.

Mats fabrication

For electrospinning ZnOnps-PCL stock solutions, adequate amounts of ZnOnps were weighted (9, 12, 15 and 25 wt.%; relative to PCL) and dispersed into AcAc. Appropriate PCL (M_n=80,000 Da, Sigma-Aldrich) amounts were incorporated (PCL 19 wt.% relative to AcAc) and nps-PCL-AcAc solutions were stirred at 300 rpm for 72 h. PCL (19 wt.% relative to AcAc) stock solutions were also prepared. Electrospinning was carried out at 17 kV using a horizontal equipment assembled in our laboratory, Supplementary Figure S1. For uniaxial-fibers mats, electrospinning solutions were ejected at 1 mL/h. For coaxial-fibers mats, the outer-shell and inner-core of a coaxial needle were filled with ZnOnps-PCL and PCL solutions, respectively, and flow rate was 0.38 mL/h. After electrospinning, mats were collected, washed with ethanol and MilliQ® water (MilliQ-H_2O) and oven-dried (36°C). Mats were named accordingly to their uniaxial- or coaxial-fiber structure and ZnOnps wt.% in electrospinning solutions, Table 1.

Table 1
Nanocomposite mats with uniaxial- or coaxial-fibers structures electrospun in the present study.

Nanocomposite mats	Composition of electrospinning solution*	
Uniaxial-fibers	**ZnO nps (wt.%)**	**PCL (wt.%)**
PCL-only	0	100
9Zn/PCL-u	9	91
12Zn/PCL-u	12	88
15Zn/PCL-u	15	85
25Zn/PCL-u	25	75
	Outer-shell	**Inner-core**
Coaxial-fibers	**ZnO nps (wt.%)/PCL (wt.%)**	**PCL (wt.%)**
9Zn/PCL-c	9 / 91	100
12Zn/PCL-c	12 / 88	100
15Zn/PCL-c	15 / 85	100
25Zn/PCL-c	25 / 75	100

Nanocomposite mats were named according to their uniaxial- or coaxial-fibers structure using the letter "u" or "c" respectively, and according to the ZnOnps concentration (wt.%) in the electrospinning ZnOnps-PCL solution used to fill the uniaxial-fibers or the outer-shell of coaxial-fibers using the number 9, 12, 15 or 25; inner-core of coaxial-fibers mats were filled with PCL solution.

* As relative to PCL and ZnOnps content only.

Mats physico-chemical characterization

Mats surface morphology was characterized by Scanning Electron Microscopy (SEM) (JEOL JSM-7800F); fibers diameter was measured from micrographs. Chemical composition was determined using Energy Dispersive X-ray Spectrometry (EDS; Oxford X-Max^{N}150) and Zn spatial distribution was characterized by EDS mapping. Coaxial- or uniaxial-fibers structures were corroborated by TEM (JEM2010 FEG). Chemical groups present were assessed by FT-IR spectroscopy and Water Contact Angles (WCA) were evaluated in static sessile drop method (Ramé-Hart Co. goniometer). X-ray Photoelectron Spectra (XPS) were acquired in a PHI Versa Probe III equipment; High Resolution Spectra (HRS) acquired in C1s, O1s and Zn2p photoelectron peaks energy regions were fitted (MultiPack Spectrum® software) to obtain surface elemental composition. Crystal structure was determined by XRD.

To evaluate Zn release, mats samples (1 mg) were incubated (37°C and 100 rpm) for 24 h in 1 mL MilliQ-H_2O. Supernatants were collected and Zn concentration was measured by Inductively Coupled Plasma Mass Spectrometry (ICP-MS; iCAP Qc, Thermo Scientific). To evaluate mats degradation, dry mats samples (8 mm-diameter) were immersed in MilliQ-H_2O, taken out, excess-water removed and weighted (W_0). Then, wet samples were incubated in 1 mL acidic medium (buffer pH=4.01, Merck) at 37°C and 100 rpm; medium was changed every 2 days. At 1, 2, 3, 6, 14 and 21 days,

samples were taken out, washed, excess-water removed and weighted (W_1). Weight loss (W_{loss}) percentage was calculated as:

$$W_{loss}[\%] = \frac{W_0 - W_1}{W_0} \times 100 \quad (2)$$

Mats antibacterial activity

It was evaluated by turbidity and MTT ([3-(4,5-dimethylthiazol-2-yl)-2,5-diphenyltetrazolium bromide]; Sigma-Aldrich) assays against *Escherichia coli* (ATCC 33780) and *Staphylococcus aureus* (ATCC 25923). The growths of pure cultures of each strain was independently collected from agar plates, resuspended in Trypticase Soy Broth (TSB, BD Bioxon) supplemented with menadione 1 v/v% and hemin 1 v/v% (Sigma-Aldrich) and adjusted to optical density = 1 at 600 nm. 300 μL of bacterial solutions were diluted in 29.7 mL of TSB to obtain ≈$1x10^7$ cells/mL. UV-sterilized mats samples (8 mm-diameter) were individually incubated at RT with 100 μL of TSB for 20 min. Two sets of mats samples were prepared; one set was illuminated with UVA light (Entela UVGL-25) during 15 min, and the other one was, meanwhile, kept in darkness. Samples in both sets were inoculated with 900 μL of bacterial solution and incubated for 24 h (35°C, natural-light illumination). Planktonic bacterial growth inhibition was estimated from absorbance of 100 μL aliquots of incubation media (turbidity assay) at 595 nm (FilterMaxF5). Bacterial cell viability (%) was calculated as:

$$\left(\frac{O.D.\ samples\ treated}{O.D.\ negative\ control}\right) \times 100 \quad (3)$$

where *O.D. samples treated* and *O.D. negative control* corresponded to absorbance of media from mats-bacteria and bacteria-only incubation, respectively. To evaluate biofilm bacterial growth inhibition, bacteria-incubated mats were rinsed with TSB, placed in clean culture-well plates and incubated with MTT:TSB solution (1:10) for 3 h at 35°C. Bacteria-metabolized formazan crystals were solubilized in *2-propanol:dimethyl sulfoxide (1:1)* and solution absorbance was read at 570 nm (FilterMax F5). Viable bacteria adhered on mats (%) was evaluated according to Eq. (3), but in this case, *O.D. samples treated* and *O.D negative control* corresponded to absorbance reads from nanocomposite and PCL-only mats, respectively. All experiments were independently performed twice for each bacterial strain tested (n=6).

Mats antibacterial activity over time was characterized using procedures described in previous paragraph but testing UVA-illuminated mats against *S. aureus* (best antibacterial results at 24 h) and evaluating planktonic and biofilm bacterial growth inhibition at 24, 48 and 72 h. Absorbance of media from bacteria-only incubation and bacteria-PCL-only MTT assays at 24 h were referenced as 100% viability for planktonic and biofilm bacterial growth, respectively. All experiments were performed by triplicate (n=3) for each evaluation time. Mats samples used for 48 h antibacterial testing were characterized by SEM to study mats stability upon antibacterial testing.

Cell response to mats

Mats capability to support cell culture and possible cytotoxicity of mats' release products were evaluated using primary human dermal fibroblast (HDF) isolated as previously described.[23] Briefly, foreskin biopsies discarded from circumcision surgeries of pediatric patients, whose parents responded to an Informed Consent approved by the INR Institutional Committee on Human Research, were obtained, fragmented and incubated with dispase II. Dermis was enzymatically digested and HDF were obtained by centrifugation, plated with supplemented-DMEM-F12 (sDMEM-F12; 1% antibiotic/antimycotic-10% fetal bovine serum) and expanded. HDF were collected, seeded (100,000 cells/cm^2) on UV-sterilized mats samples and cultured with sDMEM-F12 at 37°C and 5% CO_2. At 72 h, cell viability on mats was evaluated by fluorescence microscopy (Carl Zeiss) using the LIVE/DEAD™ Viability/Cytotoxicity Kit (Thermo Fisher). In an independent experiment, HDF were cultured on 48-wells culture plates until 80% confluence and UV-sterilized mats samples (8 mm-diameter) were incubated in 400 μL sDMEM-F12 at 37°C for 24 h. 80% confluent cell monolayers were assigned into group A or B and incubated with 100 μL mats supernatants. After 24 h, cell viability was evaluated (MTT assay) in group A. In group B, mats supernatants were replaced for fresh sDMEM-F12, monolayers were further incubated for 24 h and cell viability was assessed (MTT assay). All experiments were performed by triplicate. Control+ (ctl+) corresponded to cells cultured only with sDMEM-F12.

Statistical analysis

Results were analyzed with GraphPad Prism 5.1 software using one-way analysis of variance (ANOVA) followed by Tukey's multiple comparisons test; considering $P < 0.05$ as statistically significant.

Results

ZnO nanoparticles characterization

XRD patterns of as-received ZnOnps (Supplementary Figure S2) showed diffraction peaks corresponding to the hexagonal crystalline structure of ZnO (Zincite, JCPDS 05-0664); average crystal size was ≈22.86 nm. Crystal size corresponded to ZnOnps size as measured from TEM micrographs (≈24.33 nm), which showed hexagonal-shape nps in agreement with Zincite (Supplementary Figure S2). ZnOnps Eg was 3.21 eV (Supplementary Figure S3).

Mats physical-chemical characterization

Macroscopically, mats were ≈0.5 mm in thickness and flexible (Supplementary Figure S4). Microscopically, mats exhibited interconnected porosity and micro-fibers randomly oriented with diameters from 1.019-0.511 μm; which decreased as ZnOnps concentration in electrospinning solutions increased, Figure 1. EDS analysis (Table 2) showed high concentrations of C and O and confirmed Zn presence in nanocomposite mats, exhibiting that, coaxial-fibers mats had smaller Zn concentrations than their corresponding uniaxial-fibers mats (9Zn/PCL-u vs. 9Zn/PCL-c, 12Zn/PCL-u vs. 12Zn/PCL-c, 15Zn/PCL-u vs. 15Zn/PCL-c and 25Zn/PCL-u vs. 25Zn/PCL-c). EDS mapping showed Zn homogeneously distributed and co-localized with C and O (Figure 2, *A*). Survey XPS spectra confirmed nanocomposite mats composed by C, O and Zn in their surface and no contaminants. Fitting of HRS

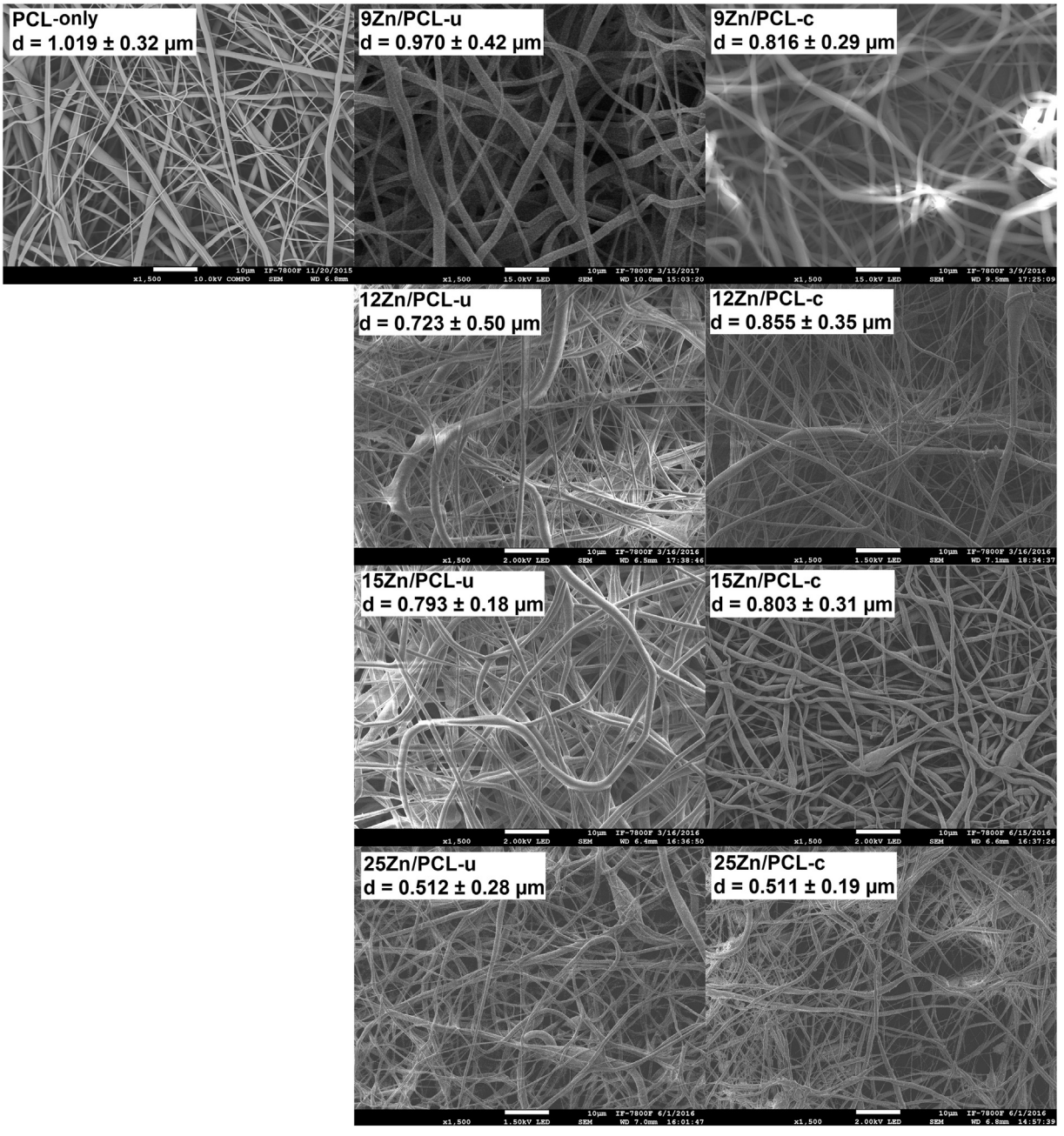

Figure 1. SEM micrographs of mats; d, mean fiber diameter.

(Supplementary Figure S5) corroborated that, in general, coaxial-fibers mats had smaller Zn concentrations than their corresponding uniaxial-fibers mats; Table 2. Deconvolution of Zn2p HRS showed Zn present only as oxidized species in their maximum valence state, Zn^{2+}. Fitting of O1s HRS evidenced Zn:O (bound to Zn) ratios slightly higher than 1:1 but smaller than 2:1.

A core-shell fiber structure in coaxial-fibers mats was confirmed from TEM micrographs, Figure 2, *B*; which also showed 20-40 nm-diameter bright nanoparticles that seemed predominantly dispersed in the outer-shell of coaxial-fibers and in the center of uniaxial-fibers. As mats Zn concentration increased, nps tended to be more clearly aligned along the axial axis of uniaxial-fibers. XRD measurements (Figure 3, *A-B*) exhibited diffraction peaks (22.54° and 24.73°) corresponding to semi-crystalline PCL.[12] Smaller intensity peaks at 31.67°, 34.19° and 35.59° were attributed to (113), (002) and (101) crystalline plane reflections of ZnO (Zincite, JCPDS 05-0664). Peaks at 20.96°, 23.88°, 28.51°, 40.31°, 41.57° and 43.00° were assigned to (111), (-112), (312), (-513), (512), (-421) crystalline plane reflections of Zn acetate (Monoclinic, JCPDS 14-902). Intensity of Zn acetate and ZnO diffraction peaks increased with mats Zn concentration. ZnO and Zn acetate average crystal sizes were 25.21 and 27.21 nm, respectively. Crystal sizes agreed with sizes of as-received ZnOnps and bright nanostructures observed in mats by TEM. FT-IR spectra (Figure 3, *C-D*) showed

Table 2
Elemental compositions of electrospun nanocomposite mats as obtained from Electron Dispersive Spectroscopy (EDS) and X-Ray Photoelectron Spectroscopy (XPS), average water contact angle (WCA) of mats and Zn release from mats as measured by Inductively Coupled Plasma Mass Spectrometry (ICP-MS).

Nanocomposite mats	Elemental composition as determined from EDS (weight %)			Elemental composition as determined from XPS (atomic %)			WCA (°)	Zn release* (ppm)
	C	O	Zn	C	O	Zn		
PCL-only	87.19	12.81	0	79	21		134.5 ± 0.7	0.00
9Zn/PCL-u	76.76	21.76	1.48	75.2	22.6	2.2	130.6 ± 0.6	48.30
12Zn/PCL-u	78.86	19.31	1.83	74.7	23.3	2.0	121.0 ± 1.3	96.52
15Zn/PCL-u	68.85	28.98	3.07	61.4	33.5	5.1	120.2 ± 0.4	98.33
25Zn/PCL-u	83.41	9.39	7.19	63.4	26.1	10.5	106.9 ± 0.4	111.30
9Zn/PCL-c	83.23	15.84	0.94	76.5	23.5	< 1	115.5 ± 0.4	58.20
12Zn/PCL-c	74.21	24.40	1.39	75.5	21.7	2.8	112.2 ± 0.5	61.65
15Zn/PCL-c	74.06	23.77	2.17	66.7	28.6	4.4	110.1 ± 1.5	78.35
25Zn/PCL-c	85.95	8.07	5.99	75.7	21.1	3.2	101.4 ± 0.4	92.20

* Zn release (ppm) corresponds to Zn concentration in supernatants after 24 h incubation of mats samples (1 mg) in 1 mL of MilliQ-water.

characteristic absorption bands of PCL at 2950 cm^{-1} ($\nu_{as}CH_2$), 2865 cm^{-1} (ν_sCH_2), 1729 cm^{-1} (ν_s-CH=O), 1294 cm^{-1} (νC-C and νC-O stretching) and 1240 cm^{-1} (ν_{as}C-O-C).[24] Nanocomposite mats did not show obvious IR bands from ZnO. The weak IR band at 1549 cm^{-1} was assigned to Zn acetate (ν_sCOO^-).[25]

WCA measurements (Supplementary Figure S6 and Table 2) showed all mats being hydrophobic (WCA>90°). PCL-only was more hydrophobic (WCA=134.5°) than nanocomposite mats (WCA≈130°-101°) and hydrophobicity decreased as Zn concentration increased; hydrophobicity decrement was higher for coaxial-fibers mats than for uniaxial-fibers mats.

Zn release in water increased as mats Zn concentration increased, independently of fiber structure (Table 2; Supplementary Figure S7). Zn release from uniaxial-fibers mats was significantly higher than that from their corresponding coaxial-fibers mats. Degradation of nanocomposite mats (in acid pH to resemble acute wounds and bacterial infection environments) significantly increased in comparison to PCL-only, Figure 3, *E-F*. Highest degradation rate occurred during the first 3 days, leading to W_{loss} of 50% and 13% for nanocomposite and PCL-only mats, respectively. After day 3, degradation rate decreased; W_{loss} at day 21 was 65% and 28% for nanocomposite and PCL-only mats, respectively. Degradation was similar for all uniaxial- and coaxial-fibers nanocomposite mats (W_{loss}=55%-68% at 21 days) independently of Zn concentration.

Antibacterial activity of mats

Capability of mats to inhibit planktonic (free-floating bacteria in media) and biofilm (adhered viable bacteria) bacterial growth was evaluated against *S. aureus* and *E. coli*. Turbidity assays after 24 h of incubation (Figure 4) indicated that nanocomposite mats significantly reduced planktonic growth in comparison to bacteria-only incubation (100% bacterial viability), for both pre-inoculation mats illumination conditions. PCL-only mats did not significantly inhibit planktonic growth. Bacterial growth decreased ≈50% in presence of nanocomposite mats for both bacterial strains tested; however, inhibition was slightly stronger against *S. aureus* than against *E. coli*. Not significant improvement of mats antibacterial activity with increasing Zn concentration was observed, independently of illumination conditions or fiber structure. 9Zn/PCL-u and 9Zn/PCL-c decreased planktonic growth by 60-50% and 50-40%, respectively for *E. coli* and *S. aureus,* and no further significant growth decrements were observed for mats with higher Zn concentration. In terms of UVA illumination effect (Figures 4, *A* vs. *B* and *C* vs. *D*), mats UVA-illuminated prior to bacteria inoculation showed improved planktonic growth inhibition against both bacteria strains tested; however, bacterial growth reduction with UVA illumination was only significant against *E. coli*, except for 12Zn/PCl-c. Under the same pre-inoculation illumination conditions, uniaxial-fibers mats exerted higher bacterial growth inhibition than their corresponding coaxial-fibers mats. Differences between antibacterial activities of corresponding uniaxial-fibers and coaxial-fibers mats against *E. coli* were significant for all Zn concentrations studied; however, significant differences were only observed for 9Zn/PCL-u vs. 9Zn/PCL-c against *S. aureus*.

Figure 5 shows percentage of viable adhered bacteria (biofilm growth) on nanocomposite mats respect to PCL-only after 24 h of mats incubation in bacterial solutions. Nanocomposite mats significantly reduced bacterial adhesion in comparison to PCL-only, for both bacterial strains tested and both pre-inoculation illumination conditions. In contrast to planktonic bacterial growth, Zn concentration played a significant role in biofilm growth reduction; general trend showed that bacterial adhesion decreased as Zn concentration increased. This was valid for both bacterial strains and both illumination conditions. Overall tendency exhibited that UVA-illuminated mats decreased bacterial adhesion, for both bacterial strains and all Zn concentrations, in comparison with mats that were kept in darkness before bacteria inoculation (Figure 5, *A* vs. *B* and *C* vs. *D*). Significant differences with UVA illumination were observed for 9Zn/PCL-c, 15Zn/PCL-u, 25Zn/PCL-u and 25Zn/PCL-c against *E. coli*, and for 9Zn/PCL-c, 12Zn/PCL-u, 12Zn/PCL-c and 25Zn/PCL-c against *S. aureus*. Under the same illumination conditions, bacterial adhesion on coaxial-fibers mats was significantly smaller than that on their corresponding uniaxial-fibers mats; even when Zn concentration was larger in uniaxial-fibers mats than in their corresponding coaxial-fibers mats.

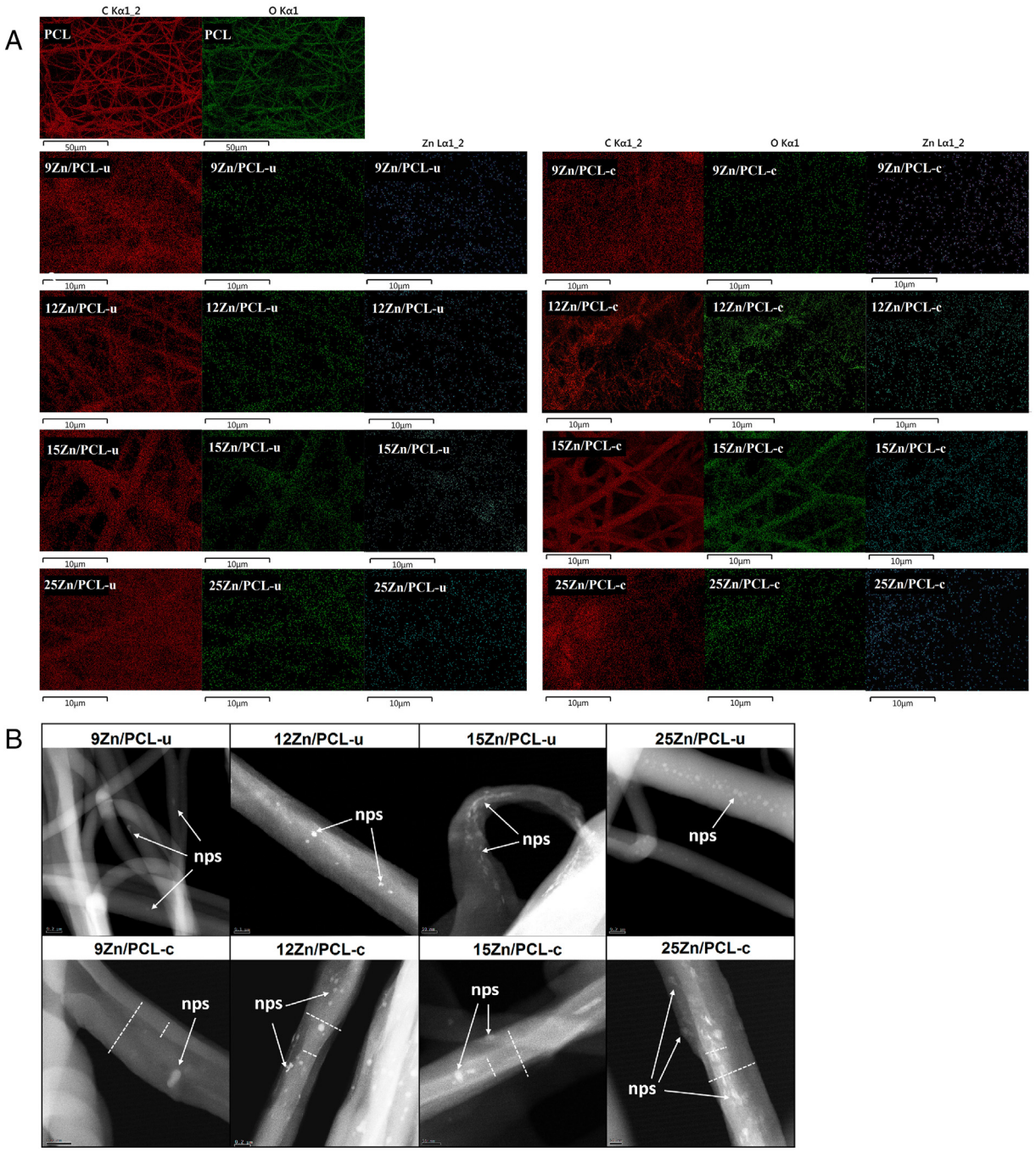

Figure 2. (**A**) Zn (blue), C (red) and O (green) EDS mapping of mats. (**B**) Representative TEM micrographs of mats.

Figure 6 shows mats antibacterial activity over time. Planktonic growth significantly increased at 48 h of incubation respect to 24 h, and at 72 h respect to 48 h, when comparing within the same nanocomposite mats (Figure 6, *A–C*), except for 15Zn/PCL-u and 25Zn/PCL-u. Nonetheless, planktonic growth in presence of nanocomposite mats (but 9Zn/PCL-c) was significantly smaller than that for ctl+ and PCL-only, at all times tested. Biofilm growth on nanocomposite mats was significantly reduced in comparison to PCL-only (Figure 6, *D–F*), at all times tested. At 48 h of mats-bacteria incubation, biofilm growth on nanocomposite mats was reduced by 60-80% in comparison to PCL-only. After 72 h, biofilm growth on nanocomposite mats, except 9Zn/PCL-u and 9Zn/PCL-c, was smaller than ≈20% the growth on PCL-only. On nanocomposite mats, no significant increment of biofilm growth (except 9Zn/PCL-u) was observed at 72 h in comparison to 24 or 48 h.

SEM characterization of mats after 48 h antibacterial testing (Supplementary Figure S8) showed bacteria adhered, slightly thicker fibers than in as-synthesized mats and, in general, mats

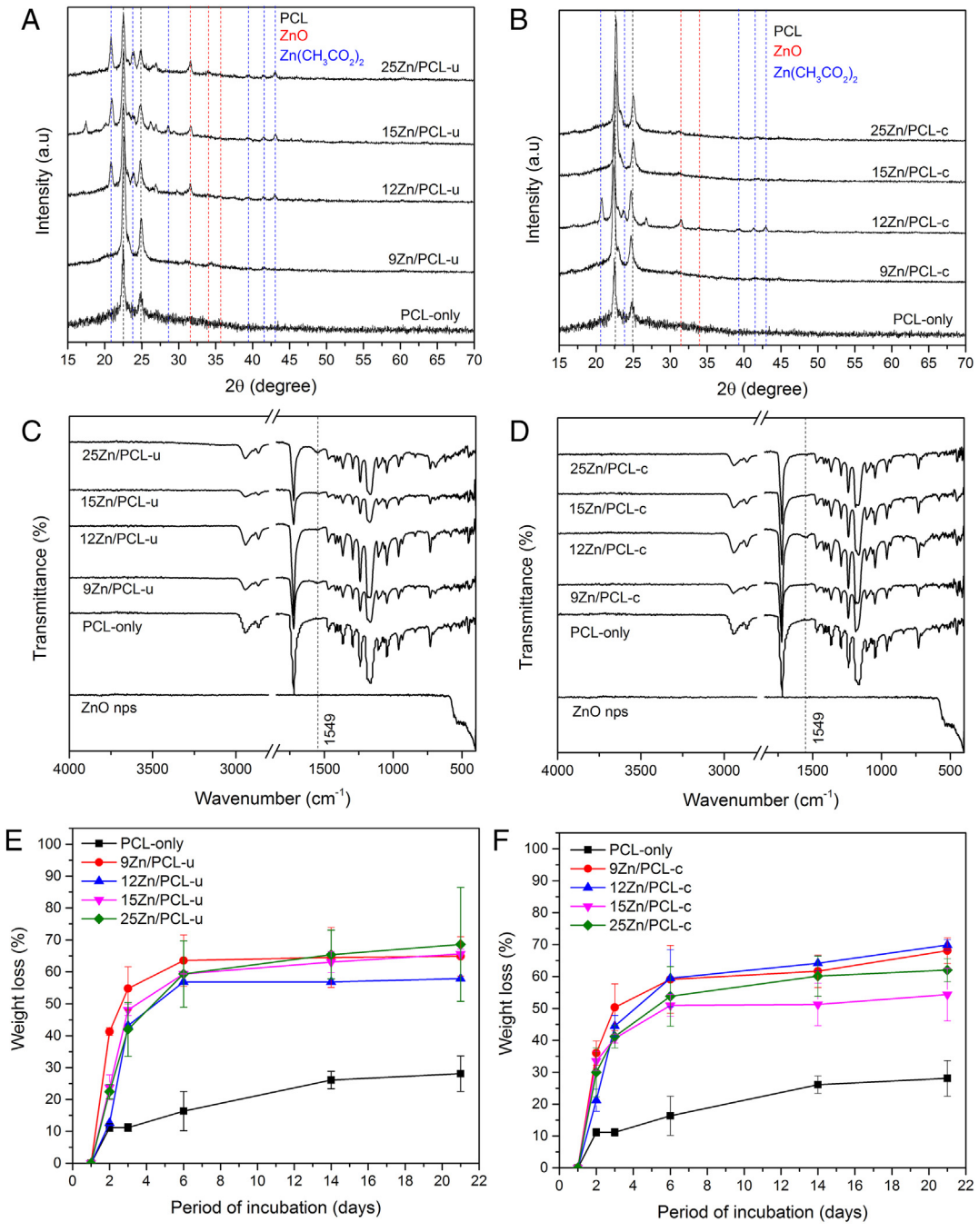

Figure 3. (**A-B**) XRD patterns of mats; semi-crystalline PCL, hexagonal ZnO and monoclinic Zn acetate diffraction peaks are marked with black, red and blue lines, respectively. (**C-D**) FT-IR spectra of mats and ZnO nanoparticles; Zn acetate $\nu_s COO^-$ band is marked. (**E-F**) Mats degradation over time in acidic medium.

morphology highly preserved. Micrographs corroborated the general trend observed for biofilm growth; bacteria adhered to mats decreased as Zn concentration increased.

HDF response to mats

Viability assays showed that nanocomposite mats did not sustain HDF culture (data not shown). HDF response to mats' release products was dependent on Zn concentration, Supplementary Figure S9, *A*). Number of metabolically active HDF (indirectly measured by the amount of cell-metabolized MTT; c-m-MTT) after 24 h of culture with mats supernatants significantly decreased as Zn concentration increased; cell culture with uniaxial-fibers mats and 25Zn/PCL-c supernatants decreased c-m-MTT by more than 50% in comparison to ctl+. C-m-MTT for HDF cultured with PCL-only supernatants was similar to ctl+. Culture with uniaxial-fibers mats supernatants reduced the number of metabolically-active cells in comparison to corresponding coaxial-fibers mats supernatants. Number of metabolically-active HDF significantly increased at 24 h after removing nanocomposite mats supernatants from cell cultures

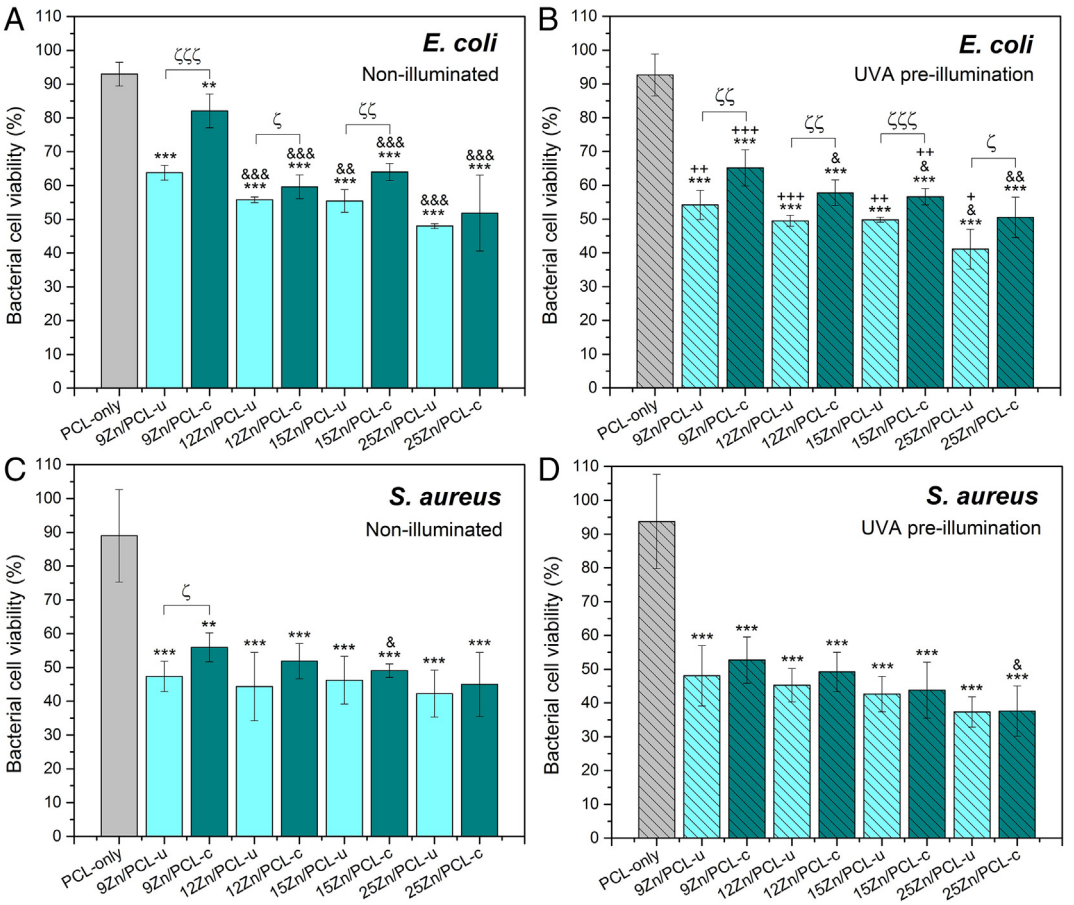

Figure 4. Planktonic bacterial growth (%) of (**A-B**) *E. coli* and (**C-D**) *S. aureus* in presence of mats, that were non-illuminated (solid bars) or UVA-illuminated (striped bars) before bacteria inoculation. *, $P < 0.05$ vs. PCL under same illumination conditions; &, $P < 0.05$ vs. mat with smallest Zn concentration and same fiber-structure under same illumination conditions; +, $P < 0.05$ non-illuminated vs. UVA-illuminated same mat; ζ, $P < 0.05$ uniaxial-fibers mats vs. corresponding coaxial-fibers mats.

(Supplementary Figure S9, *B*); c-m-MTT for HDF previously incubated with coaxial-fibers (uniaxial-fibers) mats supernatants was ≈62% (≈55%) the c-m-MTT for ctl+.

Discussion

Prevention of bacterial infection is a key step for appropriate wound treatment because bacterial infection significantly precludes wound healing.[26] Thus, in this work, coaxial and uniaxial nanocomposite Zn-based nps/PCL fibrillar mats were developed intended as potential antibacterial wound covers; with coaxial-fibers mats fabricated aiming for more efficient antibacterial materials than conventional uniaxial-fibers mats. The first step into the present study was to determine minimum Zn concentration to develop conventional uniaxial-fibers mats with significant antibacterial properties; using *E. coli* as a reference strain. Thus, uniaxial-fibers mats were electrospun from low ZnOnps concentration solutions; 3, 6, 7 and 9 wt.% relative to PCL. Significant planktonic and biofilm bacterial growth inhibition was only observed for 9 wt.% ZnOnps, Supplementary Figure S10. Therefore, 9-25 wt.% ZnOnps electrospinning solutions were studied in the present study; 25 wt.% ZnOnps reduced biofilm growth by 80% in comparison to PCL-only. Nanocomposite mats with coaxial-fibers or uniaxial-fibers structure and different Zn-based nps concentrations were successfully electrospun from ZnOnps-PCL solutions, using AcAc as a green-solvent. Mats fibers presented submicron diameters, 1.019-0.511 μm, that decreased as Zn concentration in mats increased due to the increment of charge carried by the electrospinning jet that occurs with increment of Zn-based nps concentration in electrospinning solution. Addition of ZnOnps to polymeric solutions results in higher charge densities on the jet surface during electrospinning; then, as charge carried by the jet increases with ZnOnps concentration, higher elongation forces are brought down to the jet under the electrical field, resulting in narrower fibers.[27] EDS and XPS results corroborated incorporation of higher amounts of Zn-based compounds into mats as ZnOnps concentration in electrospinning solution increased. Higher Zn concentrations were obtained in uniaxial-fibers mats, in comparison to corresponding coaxial-fibers mats, due to the PCL inner-core of coaxial-fibers decreasing the overall Zn:PCL ratio in the fibers. EDS mapping, indicated that Zn-based nps were homogeneously embedded in the fibers; an important property to conferee homogeneous antibacterial properties to mats.

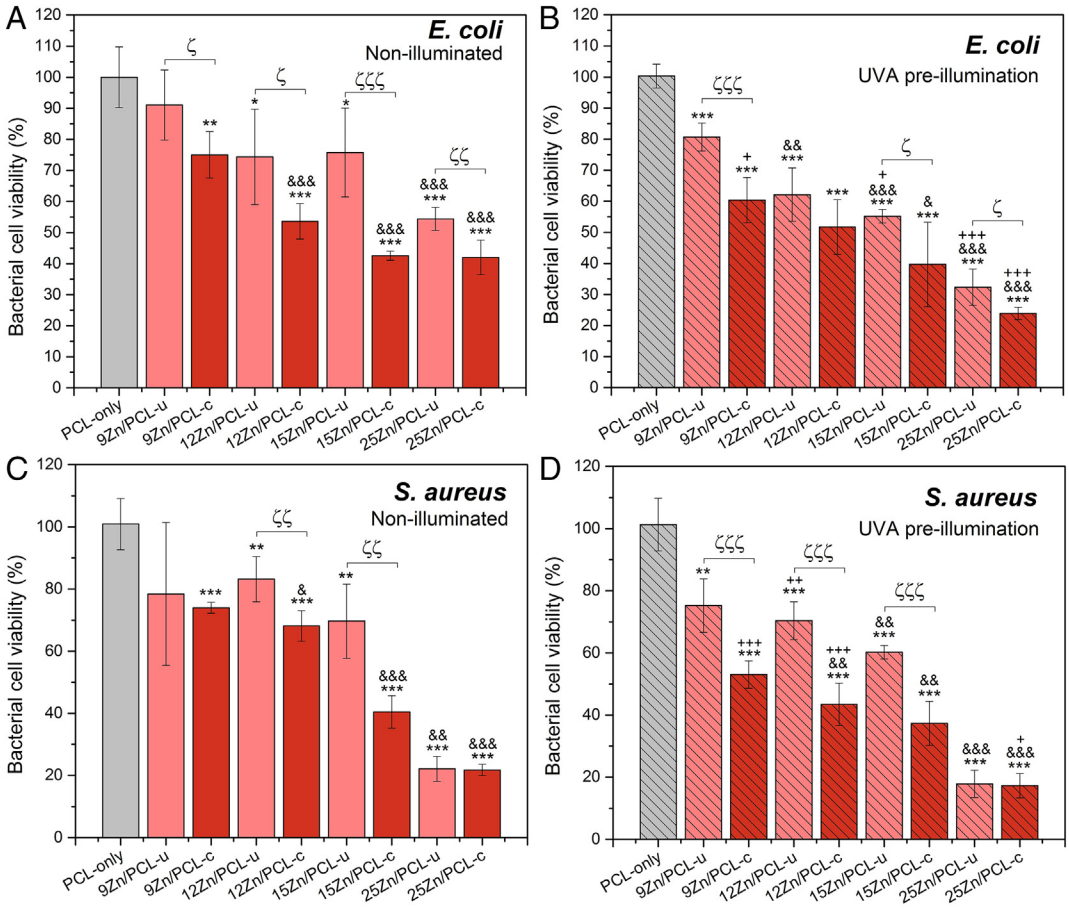

Figure 5. Biofilm bacterial growth (%) on mats incubated with (**A-B**) *E. coli* or (**C-D**) *S. aureus.* Gray, light red and dark red bars correspond to PCL-only, uniaxial-fibers and coaxial-fibers mats, respectively, that were non-illuminated (solid bars) or UVA-illuminated (striped bars) before bacteria inoculation. *, $P < 0.05$ vs. PCL under same illumination conditions; &, $P < 0.05$ vs. mat with smallest Zn concentration and same fiber-structure under same illumination conditions; +, $P < 0.05$ non-illuminated vs. UVA-illuminated same mat; ζ, $P < 0.05$ for uniaxial-fibers mats vs. corresponding coaxial-fibers mats.

Nanocomposite mats FTIR spectra did not show any clear band corresponding to Zn-O, probably because these bands were too small (small ZnOnps concentrations), plus the fact that they are expected to appear at wavenumbers <435 cm^{-1}, thus, they can easily be masked by stronger PCL vibrational modes at similar wavenumbers. The weak IR band at 1549 cm^{-1} ($\nu_s COO^-$) exhibited the formation of Zn acetate due to ZnOnps-AcAc reaction in electrospinning solutions.[25] Nevertheless, Zn acetate also possess antibacterial properties (mainly attributed to Zn^{2+} ions released upon aqueous dissolution) and has been reported as one of the most biocompatible (towards mammalian cells) antibacterial Zn salts.[19–22] Deconvolution of XPS HRS showed Zn present in mats only as oxidized species in their maximum valence state, which can correspond to ZnO or Zn acetate. Zn:O (bound to Zn) ratios were between the expected ratios for ZnO (1:1) and Zn acetate (1:2), supporting that some ZnOnps reacted with AcAc in electrospinning solutions to form Zn acetate. XRD confirmed these results, showing a mixture of nanocrystalline ZnO and Zn acetate in mats. Crystal sizes of nanocrystalline ZnO and Zn acetate agreed with dimensions of the bright nanoparticles observed by TEM, which can be confidently ascribed as Zn-based nps, since EDS and XPS mats analysis only showed C, O and Zn. Despite ZnOnps-AcAc chemical reaction, average particle size of Zn-based compounds remained in the nano-scale; probably, because ZnOnps were entrapped within the PCL polymer chains that act as particle size controller, maintaining newly formed Zn acetate particles within the nano-scale. In agreement with this, Quiros et al. reported the positive use of a low molecular weight polymer as nps size controller and capping agent for different salt precursors, including zinc acetate.[28]

TEM confirmed a coaxial-fiber structure for coaxial-fibers mats and showed that Zn-based nps were successfully embedded in coaxial-fibers and uniaxial-fibers with different distributions. During electrospinning of uniaxial fibers, PCL molecules in solution are polarized and perpendicularly aligned to the electric field; thus, the surface and center of the electrospinning jet become positively and negatively charged, respectively, and positively charged Zn-based compounds are easily attracted towards the fibers center. In the case of coaxial-fibers, the electric field is mainly generated between the external needle and the collector; hence, PCL molecules in the jet inner-core are less polarized than those in the outer-shell. Since the inner-core of coaxial-fibers is electrostatically less organized, Zn-based nps mainly remain in the outer-shell; which is advantageous because antibacterial activity highly depends on Zn-based nps surface exposure. Polar nature of Zn-based nps increased

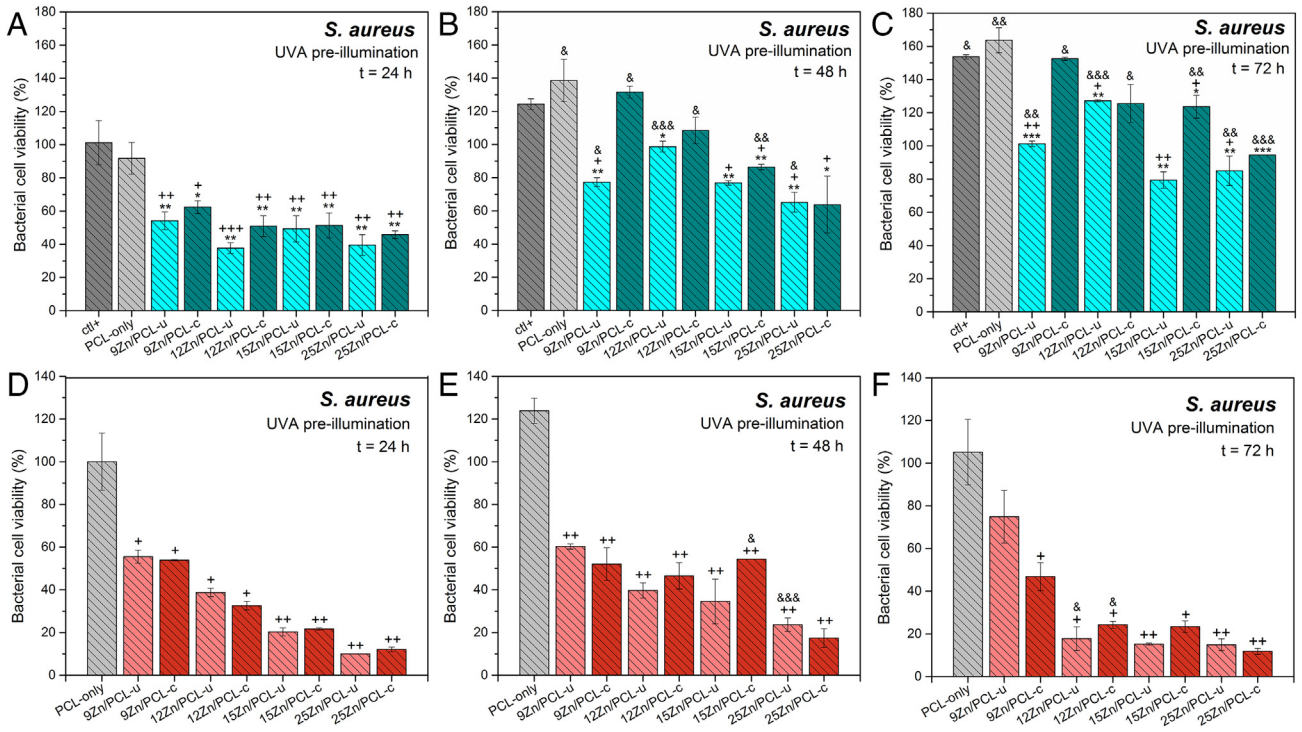

Figure 6. *S. aureus* (**A-C**) planktonic bacterial growth (%) in presence of mats or no mats (ctl+) and (**D-F**) biofilm growth (%) on mats over time. Mats samples were UVA-illuminated before bacteria inoculation. For Figures (**A–C**) *, $P < 0.05$ vs. ctl+; +, $P < 0.05$ vs. PCL; &, $P < 0.05$ vs. same mat at 24 h. For figures (**D–E**) +, $P < 0.05$ vs. PCL-only at same incubation time; &, $P < 0.05$ vs. same mat at 24 h.

water-nanocomposite mats interactions; consequently, mats hydrophobicity decreased as Zn-based nps concentration increased. Coaxial-fibers mats displayed smaller WCA than corresponding uniaxial-fibers mats, mainly due to the different distribution of Zn-based nps in coaxial and uniaxial fibers. Less hydrophobic mats might facilitate bacterial adhesion; nevertheless, antibacterial nature of ZnO and Zn acetate nps prevented this effect.

Nanocomposite mats degradation significantly increased in comparison to PCL-only, probably due to a synergistic effect of PCL degradation process and Zn-based nps properties. PCL biodegradation occurs through hydrolysis[29] and polar ZnO and Zn-acetate nps decreased mats hydrophobicity facilitating water surface interaction and consequently contributing to increase degradation. High degradation rates occurred during the first incubation days (W_{loss}=45%, day 3) and then, rates decreased (W_{loss}=65%, day 6) until no significant W_{loss} increments occurred. This degradation pattern can be explained for the first stage involving fast degradation of PCL amorphous part and the second one involving slow degradation of crystalline PCL[29,30]; Zn-based nps in mats decreased PCL crystallinity which also contribute to increase nanocomposite mats degradation in comparison to PCL-only. Mats degradation was higher than that reported by R. Augustine et al. (W_{loss}=35% at day 21) for similar membranes[30]; however, in the present work, degradation was studied at pH 4.5, while R. Augustine studied degradation at pH 7.4. As expected from mats degradation mechanisms explained, Zn release in water was dependent on, and directly correlated to, mats Zn concentration. Interestingly, for mats with small Zn concentrations (9Zn/PCL-u, 12Zn/PCL-u, 9Zn/PCL-c and 12Zn/PCL-c), Zn release seemed to be more correlated to Zn-based nps surface exposure and mats hydrophobicity than to Zn concentration, resulting in larger Zn release from coaxial-fibers mats. It was not possible to compare present Zn release with that from similar membranes previously reported (Zn release not reported)[27,30,31]; nevertheless, Zn release from present mats (0.048-0.111 mg/g) was smaller than that reported for other polymer-Zn-based membranes (≈6 mg/g).[32,33]

Antibacterial results demonstrated that, in general, mats presented slightly superior antibacterial activity against Gram-positive (*S. aureus*) than Gram-negative (*E. coli*) bacteria, in accordance with earlier reports for ZnOnps or Zn acetate.[3,21,27,34,35] This phenomenon has been commonly attributed to the fact that Gram-negative bacteria contain a lipopolysaccharides layer in the outer leaf-let of their membranes, which confers them protection against ZnO and Zn acetate. Turbidity assays showed that nanocomposite mats significantly inhibited planktonic growth against both strains tested, with uniaxial-fibers mats displaying a slightly improved effect in comparison to corresponding coaxial-fibers mats. Once mats are in culture media, fibers are widely in contact with media due to the inherent high porosity of electrospun mats; then, ZnO and, mainly, Zn acetate nps can easily release Zn^{2+} ions into media.[28] Release of Zn^{2+} ions is not expected to represent a relevant toxic factor for patients[36]; however, for unicellular organisms, such as bacteria, homeostasis can be easily compromised and Zn^{2+} can indiscriminately bind to proteins leading to Zn^{2+} intracellular accumulation and consequent bacteria dysfunction and poisoning.[37] Uniaxial-fibers mats had larger Zn concentrations and showed higher Zn release than corresponding coaxial-fibers mats, displaying improved inhibition of planktonic growth in comparison

to coaxial-fibers mats. Zn ions and ZnOnps concentrations in media similar to those determined for present mats Zn release have proved to be effectively antibacterial against *E. coli* and *S. aureus*.[21,38,39]

MTT assays showed that nanocomposite mats significantly reduced biofilm bacterial growth in comparison to PCL-only. This antibacterial effect can be mainly assigned to action of ZnOnps in mats. In support to this, improved inhibition of biofilm growth was observed on mats UVA-illuminated prior to bacteria inoculation. Effect that can be attributed to enhancement of ZnOnps photocatalytic antibacterial mechanisms upon UVA (320-400 nm) illumination; ZnO is a wide band-gap semiconductor (Eg≈3.21 eV; 386 nm) that can generate ROS in aqueous media by photocatalysis, causing bacterial oxidative stress.[40] Higher ZnOnps surface exposure could easily result in enhanced photocatalytic ROS production, explaining the enhanced biofilm growth inhibition observed on coaxial-fibers mats, in comparison to uniaxial-fibers mats. It is important to highlight that mats were UVA-illuminated for 15 min implicating that brief exposure to solar light could potentially improve mats antibacterial properties. Solar light exposure could be used as a patient-wise safe strategy to enhance or reactivate mats antibacterial properties.

Although few studies on electrospun polymeric mats using ZnOnps have been reported, R. Augustine et al. reported the development of membranes, uniaxially electrospun from 0.1-6 wt.% ZnOnps-PCL-acetone solutions, that prevented *E. coli* and *S. aureus* biofilm growth (Kirby Bauer assays); inhibition zones beyond membranes surface were only observed for samples electrospun from 5 and 6 wt.% ZnOnps polymeric solutions.[28] Actual Zn concentration in membranes was not specified but membranes EDS spectra were showed. From C:Zn EDS peaks ratios, it is possible to estimate that the highest Zn concentration studied in the present work (25Zn/PCL-u, Supplementary Figure S11) might correspond to the smallest Zn concentration membranes (1 wt.% ZnO nps-PCL-acetone solution) reported by R. Augustine.[27] In the present study significant biofilm and planktonic bacterial growth inhibition, in comparison to controls, was observed from 9Zn/PCL-c mats; Zn 0.94 wt.% as determined by EDS. Thus, present mats prevented bacterial adhesion in a similar way to those previously reported by R. Augustine, but also inhibited bacterial planktonic growth. E.A. Münchow et al. also reported the development of antibacterial ZnO-loaded electrospun membranes, observing inhibition halos dependent on membranes Zn concentration[35]; average Zn incorporation in membranes reported (≈Zn 3.04 wt.%) were higher than those of mats in the present study, except for 25Zn/PCL-c and 25Zn/PCL-u. Nevertheless, bacterial strains tested by E.A. Münchow differed from present bacterial strains tested.[31]

Nanocomposite mats antibacterial activity last for up to 3 days and mats degradation was not significant upon antibacterial testing; however, nanocomposite mats did not sustain HDF culture. Thus, mats have not potential application as tissue regeneration-intended materials or scaffolds but as antibacterial covers that could be applied on top of tissue regeneration-intended scaffolds or skin substitutes. Considering this latter application, one of the main concerns might be then, the release of Zn-based compounds into host tissue. *In-vitro* results showed that upon HDF incubation with nanocomposite mats supernatants, the number of metabolically active cells decreased in comparison to controls, in agreement with previous reports of Zn release effects on cells.[41–43] Nevertheless, HDF recovered their metabolic activity upon elimination of mats supernatants. Zn concentrations measured in mats supernatants (43.48-111.43 ppm) were significantly higher than physiological Zn concentrations in saliva[20] but close to therapeutic daily Zn dosages (≈58 ppm),[44] and smaller than Zn concentrations in treatments successfully applied dermatologically without causing significant adverse effects in humans.[45] Moreover, Zn-based nps LC_{50} dosages for small invertebrates have been showed to be 1.79-67.97 ppm[46]; thus, Zn release from nanocomposite mats are not expected to be potentially harmful for humans.

In general, enhanced and patient-wise possibly less toxic antibacterial coaxial-fibers nanocomposite mats were developed, constituting materials with capability to prevent planktonic and biofilm bacterial growth and promising applications as temporarily wound covers.

Acknowledgements

The authors acknowledge the technical support of R. Hernández, D. Quiterio (TEM and SEM), M. Canseco (FT-IR), A. Tejeda (XRD) and L. Huerta (XPS) from Universidad Nacional Autónoma de México (UNAM), and A. D. Hernández (TEM characterization of Zn-based nps) from Instituto Nacional de Rehabilitación Luis Guillermo Ibarra Ibarra.

Appendix A. Supplementary data

Supplementary data to this article can be found online at https://doi.org/10.1016/j.nano.2018.04.005.

References

1. Ventola CL. The antibiotic resistance crisis: part 1: causes and threats. *P T* 2015;**40**(4):277-83.
2. WHO. *Global Report on Surveillance: Antimicrobial Resistance*. World Heal. Organ.; 20141-7.
3. Pati R, Mehta RK, Mohanty S, Padhi A, Sengupta M, Vaseeharan B, et al. Topical application of zinc oxide nanoparticles reduces bacterial skin infection in mice and exhibits antibacterial activity by inducing oxidative stress response and cell membrane disintegration in macrophages. *Nanomedicine* 2014;**10**(6):1195-208.
4. Salem W, Leitner DR, Zingl FG, Schratter G, Prassl R, Goessler W, et al. Antibacterial activity of silver and zinc nanoparticles against Vibrio cholerae and enterotoxic Escherichia coli. *Int J Med Microbiol* 2015;**305**(1):85-95.
5. Sarwar S, Chakraborti S, Bera S, Sheikh IA, Hoque KM, Chakrabarti P. The antimicrobial activity of ZnO nanoparticles against Vibrio cholerae: Variation in response depends on biotype. *Nanomedicine* 2016;**12**(6):1499-509.
6. He W, Jia H, Cai J, Han X, Zheng Z, Wamer WG, et al. Production of Reactive Oxygen Species and Electrons from Photoexcited ZnO and ZnS Nanoparticles: A Comparative Study for Unraveling their Distinct Photocatalytic Activities. *J Phys Chem C* 2016;**120**(6):3187-95.
7. Sultana S, Rafiuddin, Khan MZ, Shahadat M. Development of ZnO and ZrO<inf>2</inf> nanoparticles: Their photocatalytic and bactericidal activity. *J Environ Chem Eng* 2015;**3**(2):886-91.
8. Guo B-L, Han P, Guo L-C, Cao YQ, Li AD, Kong JZ, et al. The Antibacterial Activity of Ta-doped ZnO Nanoparticles. *Nanoscale Res Lett* 2015;**10**(336):1-10.

9. Stankic S, Suman S, Haque F, Vidic J. Pure and multi metal oxide nanoparticles: synthesis, antibacterial and cytotoxic properties. *J Nanobiotechnol* 2016;**14**(1):73.
10. Qian Y, Zhang Z, Zheng L, Song R, Zhao Y. Fabrication and Characterization of Electrospun Polycaprolactone Blended with Chitosan-Gelatin Complex Nanofibrous Mats. *J Nanomater* 2014;**2014**:1-7.
11. EMEA. ICH guideline Q3C (R6) on impurities: guideline for residual solvents. *Int Conf Harmon* 2003;**68**(December 2016):1-35.
12. Ferreira JL, Gomes S, Henriques C, Borges JP, Silva JC. Electrospinning polycaprolactone dissolved in glacial acetic acid: Fiber production, nonwoven characterization, and In Vitro evaluation. *J Appl Polym Sci* 2014;**41068**:37-9.
13. Ip M, Lui SL, Poon VKM, Lung I, Burd A. Antimicrobial activities of silver dressings: An in vitro comparison. *J Med Microbiol* 2006;**55**(1):59-63.
14. Mama M, Abdissa A, Sewunet T. Antimicrobial susceptibility pattern of bacterial isolates from wound infection and their sensitivity to alternative topical agents at Jimma University Specialized Hospital, South-West Ethiopia. *Ann Clin Microbiol Antimicrob* 2014;**13**(1):14.
15. Moş I, Micle O, Zdrâncă M, Mureşan M, Vicaş L. Antibiotic sensitivity of the Escherichia coli strains isolated from infected skin wounds. *Farmacia* 2010;**58**(5):637-45.
16. Aktar T, Towhid ST, Islam KMS, Fatema K, Islam S, Majumder P, et al. Bacterial skin and soft tissue infection in Dhaka, Bangladesh. *IOSR J Pharm Biol Sci Ver III* 2015;**10**(2):2319-7676.
17. Giacometti A, Cirioni O, Schimizzi AM, Del Prete MS, Barchiesi F, D'Errico MM, et al. Epidemiology and Microbiology of Surgical Wound Infections Epidemiology and Microbiology of Surgical Wound Infections. 2000;**38**(2):918-22.
18. Shoeb M, Singh BR, Khan JA, Khan W, Naqvi AH, Singh BN, et al. ROS-dependent anticandidal activity of zinc oxide nanoparticles synthesized by using egg albumen as a biotemplate. *Nat Sci Nanosci Nanotechnol* 2013;**4**(35015):1-11.
19. Chandra RGS, Ramesh TN, Veeranna VG, Maiya PS. Antimicrobial activity studies of zinc oxide, zinc acetate and layered zinc hydroxysalt. 2014;**1**(January 2013):524-30.
20. Burguera-Pascu M, Rodríguez-Archilla A, Baca P. Substantivity of zinc salts used as rinsing solutions and their effect on the inhibition of Streptococcus mutans. *J Trace Elem Med Biol* 2007;**21**(2):92-101.
21. Atmaca S, Gül K, Çiçek R. The effect of zinc on microbial growth. *J iMed Sci* 1998;**28**:595-7.
22. Pavlica S, Gaunitz F, Gebhardt R. Comparative in vitro toxicity of seven zinc-salts towards neuronal PC12 cells. *Toxicol In Vitro* 2009;**23**(4):653-9.
23. Velasquillo C, Silva-Bermudez P, Vázquez N, Martínez A, Espadín A, García-López J, et al. In vitro and in vivo assessment of lactic acid-modified chitosan scaffolds for potential treatment of full-thickness burns. *J Biomed Mater Res A* 2017;**105**(10):2875-91.
24. Prasad T, Shabeena EA, Vinod D, Kumary TV, Anil Kumar PR. Characterization and in vitro evaluation of electrospun chitosan/polycaprolactone blend fibrous mat for skin tissue engineering. *J Mater Sci Mater Med* 2015;**26**(1):1-13.
25. Zhang Y, Zhu F, Zhang J, Xia L. Converting layered zinc acetate nanobelts to one-dimensional structured ZnO nanoparticle aggregates and their photocatalytic activity. *Nanoscale Res Lett* 2008;**3**(6):201-4.
26. Church D, Elsayed S, Reid O, Winston B, Lindsay R. Burn wound infections. *Clin Microbiol Rev* 2006;**19**(2):403-34.
27. Augustine R, Malik HN, Singhal DK, Mukherjee A, Malakar D, Kalarikkal N, et al. Electrospun polycaprolactone/ZnO nanocomposite membranes as biomaterials with antibacterial and cell adhesion properties. *J Polym Res* 2014;**21**(3):347.
28. Mater JH, Quirós J, Borges JP, Boltes K, Rosal R. Antimicrobial electrospun doped polyvinylpyrrolidone nanofibers. 2015;**299**(December):298-305.
29. Woodruff MA, Hutmacher DW. *Prog Polym Sci* 2010;**35**(10):1217-56 [Internet, Available from: https://www.sciencedirect.com/science/article/pii/S0079670010000419?via%3Dihub].
30. Augustine R, Kalarikkal N, Thomas S. Effect of zinc oxide nanoparticles on the in vitro degradation of electrospun polycaprolactone membranes in simulated body fluid. *Int J Polym Mater Polym Biomater* 2016;**65**(1):28-37.
31. Münchow EA, Albuquerque MTP, Zero B, Kamocki K, Piva E, Gregory RL, et al. Development and characterization of novel ZnO-loaded electrospun membranes for periodontal regeneration. *Dent Mater* 2015;**31**(9):1038-51.
32. Liu P, Zhao M. Silver nanoparticle supported on halloysite nanotubes catalyzed reduction of 4-nitrophenol (4-NP). *Appl Surf Sci* 2009;**255**(7):3989-93.
33. Ashfaq M, Verma N, Khan S. Highly effective Cu/Zn-carbon micro/nanofiber-polymer nanocomposite-based wound dressing biomaterial against the P aeruginosa multi- and extensively drug-resistant strains. *Mater Sci Eng C* 2017;**77**:630-41 [Internet, Available from: https://doi.org/10.1016/j.msec.2017.03.187].
34. Premanathan M, Karthikeyan K, Jeyasubramanian K, Manivannan G. Selective toxicity of ZnO nanoparticles toward Gram-positive bacteria and cancer cells by apoptosis through lipid peroxidation. *Nanomedicine* 2011;**7**(2):184-92.
35. Brayner R, Ferrari-Iliou R, Brivois N, Djediat S, Benedetti MF, Fiévet F. Toxicological impact studies based on *Escherichia coli* bacteria in ultrafine ZnO nanoparticles colloidal medium. *Nano Lett* 2006;**6**(4):866-70.
36. Maret W. The metals in the biological periodic system of the elements: concepts and conjectures. *Int J Mol Sci* 2016;**17**(1):1-8.
37. Lemire JA, Harrison JJ, Turner RJ. Antimicrobial activity of metals: mechanisms, molecular targets and applications. *Nat Rev Microbiol* 2013;**11**(6):371-84.
38. Kumar R, Umar A, Kumar G, Nalwa HS. Antimicrobial properties of ZnO nanomaterials: A review. *Ceram Int* 2017;**43**(5):3940-61.
39. Pati R, Mehta RK, Mohanty S, Padhi A, Sengupta M, Vaseeharan B, et al. Topical application of zinc oxide nanoparticles reduces bacterial skin infection in mice and exhibits antibacterial activity by inducing oxidative stress response and cell membrane disintegration in macrophages. *Nanomedicine* 2014;**10**(6):1195-208 [Internet, Available from: https://doi.org/10.1016/j.nano.2014.02.012].
40. Cabiscol E, Tamarit J, Ros J. Oxidative stress in bacteria and protein damage by reactive oxygen species. *Int Microbiol* 2011;**3**(1):3-8.
41. Pavlica S, Gaunitz F, Gebhardt R. Comparative in vitro toxicity of seven zinc-salts towards neuronal PC12 cells. *Toxicol In Vitro* 2009;**23**(4):653-9 [Internet, Available from: https://doi.org/10.1016/j.tiv.2009.03.003].
42. Uski O, Torvela T, Sippula O, Karhunen T, Koponen H, Peräniemi S, et al. In vitro toxicological effects of zinc containing nanoparticles with different physico-chemical properties. *Toxicol In Vitro* 2017;**42**(September 2016):105-13 [Internet, Available from: https://doi.org/10.1016/j.tiv.2017.04.010].
43. Kaur P, Thakur R, Barnela M, Chopra M, Manuja A, Chaudhury A. Synthesis, characterization and *in vitro* evaluation of cytotoxicity and antimicrobial activity of chitosan-metal nanocomposites. *J Chem Technol Biotechnol* 2015;**90**(5):867-73 [Internet, Available from: http://doi.wiley.com/10.1002/jctb.4383].
44. Cipriano AF, Zhao T, Johnson I, Guan RG, Garcia S, Liu H. In vitro degradation of four magnesium-zinc-strontium alloys and their cytocompatibility with human embryonic stem cells. *J Mater Sci Mater Med* 2013;**24**(4):989-1003.
45. Gupta M, Mahajan VK, Mehta KS, Chauhan PS. Zinc therapy in dermatology: A review. *Dermatol Res Pract* 2014;**709152**:1-11.
46. Hou J, Wu Y, Li X, Wei B, Li S, Wang X. Toxic effects of different types of zinc oxide nanoparticles on algae, plants, invertebrates, vertebrates and microorganisms. *Chemosphere* 2018;**193**:852-60 [Internet, Available from: https://doi.org/10.1016/j.chemosphere.2017.11.077].